DENTAL MATERIALS 35 (2019) 156–168

Available online at www.sciencedirect.com

ScienceDirect

journal homepage: www.intl.elsevierhealth.com/journals/dema

Antibacterial effects of polymeric PolymP-*n* Active nanoparticles. An *in vitro* biofilm study

M.C. Sánchez[a], *M. Toledano-Osorio*[b], *J. Bueno*[a], *E. Figuero*[a], *M. Toledano*[b], *A.L. Medina-Castillo*[c], *R. Osorio*[b,*], *D. Herrera*[a], *M. Sanz*[a]

[a] *ETEP (Etiology and Therapy of Periodontal Diseases) Research Group, University Complutense, Madrid, Spain*
[b] *Biomaterials in Dentistry Research Group, University of Granada, Spain*
[c] *NanoMyP. Spin-Off Enterprise from University of Granada, Edificio BIC-Granada, Av. Innovación 1, 18016 Armilla, Granada, Spain*

ARTICLE INFO

Article history:
Received 7 September 2018
Received in revised form
8 November 2018
Accepted 9 November 2018

Keywords:
Oral biofilm
Nanoparticles
Doxycycline
Calcium
Zinc
Silver

ABSTRACT

Objective. to study the antibacterial effect of polymeric PolymP-*n* Active nanoparticles using an *in vitro* subgingival biofilm model.

Methods. Hydroxyapatite discs coated with five modalities of nanoparticles (NPs): NPs, NPs doped with zinc, calcium, silver and doxycycline, PBS as control, and *Streptococcus oralis*, *Actinomyces naeslundii*, *Veillonella parvula*, *Fusobacterium nucleatum*, *Porphyromonas gingivalis* and *Aggregatibacter actinomycetemcomitans* were studied in a static *in vitro* biofilm model (12, 24, 48, and 72 h). Nano-roughness of the different disc surfaces (SRa, in nm) and morphological characteristic of the biofilms (thickness (μm) and bacterial viability) were studied by different microscopy modalities. Quantitative Polymerase Chain Reaction was used to assess the effect of the nanoparticles on the bacterial load (colony forming unit per milliliter) (CFU mL^{-1}). Analysis of variance and post-hoc testing with T3 Dunnett´s, and Student Newman Keuls correction was used. Results were considered statistically significant at $p < 0.05$.

Results. Surfaces containing the different nanoparticles showed significant increments in roughness when compared to controls ($p < 0.05$). A similar biofilm formation and dynamics was observed, although reductions in bacterial viability were detected in biofilms in contact with the different nanoparticles, more pronounced with silver and doxycycline NPs. Doxycycline-NPs biofilms resulted in unstructured biofilm formation and significantly lower number of the six species when compared with the other nanoparticles specimens and controls ($p < 0.001$ in all cases).

Significance. Polymeric PolymP-*n* Active nanoparticles when combined with silver and doxycycline showed a significant antibacterial effect when tested in an *in vitro* subgingival biofilm model.

* *Corresponding author at*: Dental School, University of Granada, Colegio Maximo, Campus de Cartuja s/n, 18017 Granada, Spain.
E-mail address: rosorio@ugr.es (R. Osorio).

https://doi.org/10.1016/j.dental.2018.11.015

1. Introduction

Periodontitis is a chronic inflammatory disease characterized by destruction of the tooth supporting structures (cementum, periodontal ligament and bone) and if untreated may lead to tooth loss. Periodontal therapy is mainly aimed to the reduce or eliminate the subgingival biofilm in order to arrest the inflammatory condition and, in specific periodontal lesions or defects different regenerative surgical interventions, have demonstrated a high degree of predictability in the regeneration of the lost periodontal structures within the confines of the lesion [1].

Periodontal regeneration, however, require a complex interaction of biological events occurring during postoperative healing. These factors include the availability of the adequate cell source, molecular mediators and appropriate scaffold for space maintenance, in an environment with an adequate blood supply and absence of inflammation [2]. Since wound healing of periodontal regenerative surgical interventions will occur in a transmucosal environment, infection control will become a key factor in inflammation control and in the achievement of the regenerative outcomes [3,4].

While mechanical plaque control is hampered during the early postoperative period, the use of local and systemic antibiotics, together with the application of topical antiseptics, mainly in the form of mouth rinses, has been the main therapy for infection control, demonstrating heterogeneous results [4–7]. These variable outcomes may be due to different factors, such as the quality of the surgical intervention, the biomaterials used, the capacity of the antimicrobial product to reach the area, its bioavailability and concentration at the regenerative site, etc. [1].

One possible alternative for infection control has been the design and development of biocompatible and non-reabsorbable nanoparticles, which may achieve high local bioactivity and slowly release antibacterial effects [8,9]. This technology has been recently used in periodontal regeneration [10,11], dental re-naturalization, local anesthesia or treatment of dentin hypersensitivity [12,13]. In this field, a novel type of polymeric nanoparticles, PolymP-*n* Active nanoparticles (NPs) has been recently developed by Osorio et al., with potential for periodontal regeneration [11,14,15]. Due to the surface chemistry of the NPs, containing functional groups with sequences of anionic carboxylate (i.e. COO-), it was possible to dope metal cations (in this case calcium, zinc and silver) and antibiotics (doxycycline), with potential antibacterial activity. The use of metals, such as silver and zinc, complexed on nanoparticles have demonstrated anti-infective properties and have been used in commercial products with different applications [16–19]. Doxycycline is a well-known broad-spectrum antibiotic, which has been formulated for controlled delivery, demonstrating long-term inhibition of bacterial growth [20–22].

It was, therefore, the aim of this investigation to study the possible antibacterial effect of polymeric PolymP-*n* Active nanoparticles (NPs) doped with different substances: zinc, calcium, silver and doxycycline, on a validated *in vitro* oral biofilm model [23].

2. Material and methods

2.1. Bacterial strains and culture conditions

Reference strains *Streptococcus oralis* CECT 907T, *Veillonella parvula* NCTC 11810, *Actinomyces naeslundii* ATCC 19039, *Fusobacterium nucleatum* DMSZ 20482, *Aggregatibacter actinomycetemcomitans* DSMZ 8324 and *Porphyromonas gingivalis* ATCC 33277 were used. Bacteria were grown on blood agar plates (Blood Agar Oxoid N° 2; Oxoid, Basingstoke, UK), supplemented with 5% (v/v) sterile horse blood (Oxoid), 5.0 mg L^{-1} hemin (Sigma, St. Louis, MO, USA) and 1.0 mg L^{-1} menadione (Merck, Darmstadt, Germany) in anaerobic conditions (10% H_2, 10% CO_2, and balance N_2) at 37 °C for 24–72 h.

2.2. Nanoparticles fabrication

Five different nanoparticles have been subjected to study: (a) PolymP-*n* Active nanoparticles (NPs) developed as previously described by Osorio et al. [11]; (b) NPs doped with zinc (Zn-NPs); (c) with calcium (Ca-NPs); (d) with silver (Ag-NPs); and (e) with doxycycline (Doxy-NPs). These PolymP-*n* Active nanoparticles with a diameter of 100 nm were fabricated through a polymerization/precipitation process with a composition of 2-hydroxyethyl methacrylate (backbone monomer), ethylene glycol dimethacrylate (cross-linker) and methacrylic acid (functional monomer). For the doping process with zinc, calcium and silver, 30 mg of NPs were immersed during 3 days at room temperature, and under continuous agitation, in an aqueous solution of $ZnCl_2$, $CaCl_2$ or NO_3Ag (containing zinc, calcium and silver at 40 ppm at pH 6.5) until reaching the adsorption equilibrium of metal ions [11]. Then, by centrifugation (20 min, 4 °C, 8,000x*g*), the particles were separated from the supernatant and suspended in phosphate buffered saline (PBS). For doping NPs with doxycycline, 30 mg of NPs were immersed in a 40 mg ml^{-1} aqueous solution of doxycycline hyclate, during 4 hours at room temperature and under continuous shaking [24]. Then, the suspensions were centrifuged (20 min, 4 °C, 8,000x*g*), the particles separated from the supernatant and suspended in PBS. Doxy-NPs were used 7 days after loading, in order to avoid the initial burst of doxycycline liberation [24].

2.3. Saliva preparation

Unstimulated saliva was obtained from healthy volunteers in 10 mL aliquots at least 1.5 h after eating, drinking or tooth brushing. Each saliva sample was treated with 2.5 mmol L^{-1} DL-Dithiothreitol (Sigma) for 10 min with continuous stirring in order to reduce salivary protein aggregation. It was then centrifuged (10 min, 4 °C, 9,000x*g*) and the obtained supernatant diluted (1:1) with PBS. The sample was then filtered and sterilized through a 0.22 μm pore size Millex GV low-protein-binding filter X50 (Millipore, Millipore Corporation Bedford, USA) and stored at −20 °C. The efficacy of this protocol was assessed by plating processed saliva samples onto supplemented blood agar plates for 72 h at 37 °C and confirming the lack of any bacterial growth on either aerobically or anaerobically incubated plates.

2.4. Preparation of the specimens

Sterile calcium hydroxyapatite (HA) discs with a 7 mm of diameter and a thickness 1.8 mm (standard deviation, SD = 0.2) (Clarkson Chromatography Products, Williamsport, PA, USA) were immersed in the treated saliva for 4 h at 37 °C in sterile plastic tubes. Then, HA discs were coated on their surfaces with one of the five types of NPs, depositing 50 μL of each nanoparticle suspension (10 mg mL^{-1}) [24], in a laminar flow chamber under sterile condition at room temperature. The HA discs were considered as coated with the nanoparticles on the surface when the evaporation of the suspension was complete (1 h approximately). Discs coated with PBS were used as controls.

2.5. Nano-roughness analysis of surfaces

Three specimens of each NPs-coated HA discs and negative controls were observed under Atomic Force Microscopy (AFM) to evaluate their topography and nano-roughness. The AFM imaging process (Nanoscope V, Digital Instruments, Veeco Metrology group, Santa Barbara, CA, USA) was used in the tapping mode, with a calibrated vertical-engaged piezo-scanner. A 10-nm-radius silicon nitride tip was attached to the end of an oscillating cantilever put in intermittent contact with the surface at the lowest point of the oscillation. Changes in vertical position of the AFM tip at resonance frequencies near 330 kHz provided the height of the images registered as bright and dark regions. Three 10 × 10 μm digital images were recorded from each surface, with a slow scan rate (0.1 Hz). Measurements were performed in a wet cell, under hydrated conditions. For each image, five randomized boxes (2 μm × 2 μm) were created to determine surface nano-roughness (SRa, in nm).

2.6. Biofilm development

The HA discs loaded with the nanoparticles and the controls were used to develop a multispecies oral biofilm, as previously described by Sánchez et al. [23]. In brief, pure cultures of each bacterium were grown anaerobically in a protein-rich medium containing brain-heart infusion (BHI) (Becton, Dickinson and Company, Franklin Lakes, NJ, USA) supplemented with 2.5 g L^{-1} mucin (Oxoid), 1.0 g L^{-1} yeast extract (Oxoid), 0.1 g L^{-1} cysteine (Sigma), 2.0 g L^{-1} sodium bicarbonate (Merck), 5.0 mg L^{-1} hemin (Sigma, St. Louis, MO, USA) and 1.0 mg L^{-1} menadione (Merck, Darmstadt, Germany) and 0.25% (v/v) glutamic acid (Sigma). The bacterial growth was harvested at mid-exponential phase (measured by spectrophotometry), and a mixed bacteria suspension in modified BHI medium containing 10^3 colony forming units (CFU) mL^{-1} for *S. oralis*, 10^5 CFU mL^{-1} for *V. parvula* and *A. naeslundii*, and 10^6 CFU mL^{-1} for *F. nucleatum, A. actinomycetemcomitans* and *P. gingivalis* was prepared.

HA discs coated with PBS or with the different NPs were then placed in the wells of a 24-well tissue culture plate (Greiner Bio-one, Frickenhausen, Germany). Each well was then inoculated with 1.5 mL mixed bacteria suspension prepared, and incubated in anaerobic conditions (10% H_2, 10% CO_2, and balance N_2) at 37 °C for 12, 24, 48 and 72 h. Plates containing only culture medium will be also incubated to check for sterility.

2.7. Morphological analysis of the biofilms

Biofilms from 12 to 72 h of evolution were observed by Scanning Electron Microscopy (SEM). For this analysis, the specimens were fixed in a solution at 4% paraformaldehyde and 2.5% glutaraldehyde for 4 h at 4 °C. The discs were washed once in PBS, then in sterile water for 10 min and then dehydrated through a series of graded ethanol solutions (30, 50, 70, 80, 90 and 100%; immersion time per series 10 min). After that, specimens were critical point dried, sputter-coated with gold and analysed by electron microscopy using a JSM 6400 (JSM6400; JEOL, Tokyo, Japan), with a back-scattered electron detector and an image resolution of 25 kV. Also, selected specimens were carbon-coated and observed by Field Emission Electron Microscopy (FESEM) (GEMINI, Carl Zeiss SMT, Germany) at 3 kV.

2.8. Biofilm Vitality

Vitality of mature biofilms (72 h) was studied by Confocal Laser Scanning Microscopy (CLSM). Non-invasive confocal imaging of fully hydrated biofilms was obtained by means of a fixed-stage Ix83 Olympus inverted microscope coupled to an Olympus FV1200 confocal system (Olympus; Shinjuku, Tokio, Japan). The objective lens was a × 63 water-immersion lens (Olympus). Specimens were stained with LIVE/DEAD® BacLight™ Bacterial Viability Kit solution (Molecular Probes B. V., Leiden, The Netherlands) at room temperature. A 1:1 fluorocromes ratio and 9 ± 1 min of staining time was used to obtain the optimum fluorescence signal at the corresponding wave lengths (Syto9: 515–530 nm; PI: >600 nm). The CLSM control software was set to take a z-series of scans (xyz) of 0.5 μm thickness (8 bits, 1024 × 1024 pixels). Three specimens were analyzed and representative locations on the HA discs covered with biofilm, which contained stacks (or "towers") that could be isolated within the confocal view field, were selected for these measurements. Within each area, the thickest point was measured by determination of the upper and lower boundaries of the biofilm. Image stacks were analyzed using the microscope dedicated software (Olympus®). To quantify the biomass and cell viability within the biofilm, total fluorescent staining of the confocal micrographs was analyzed using an image analysis software (Imaris® Biteplane, Belfast, UK), by measuring voxel intensities from two-channel images, and thus calculating the percentage of the biomass and cell viability within the stacks. Fluorescence intensity thresholds were manually set for each of the fluorescent color.

2.9. Biofilm biomass and quantitative evaluation of bacteria

Biofilm DNA, of 12, 24, 48 and 72 h of growth was isolated using a commercial kit (MolYsis Complete5; Molzym GmgH & CoKG, Bremen, Germany), following manufacturer's instructions (the protocol for bacterial DNA extraction was followed from step 6, avoiding preliminary steps). The hydrolysis probe 5′nuclease assay PCR method was used for detecting and quantifying

the bacterial DNA. Primers and probes were obtained by Life Technologies Invitrogen (Carlsbad, CA, USA), Applied Biosystems (Carlsbad, CA, USA) and Roche (Roche Diagnostic GmbH; Mannheim, Germany) and were targeted against 16S rRNA gene [25]. The quantitative Polymerase Chain Reaction (qPCR) amplification was performed in a total reaction mixture volume of 10 μL. The reaction mixtures contained 5 μL of 2x master mixture (LC 480 Probes Master; Roche), optimal concentrations of primers and probe (900, 900 and 300 nM for *S. oralis*; 300, 300 and 300 nM for *A. naeslundii*; 750, 750 and 400 nM for *V. parvula*; 300, 300 and 200 nM for *A. actinomycetemcomitans*; 300, 300 and 300 nM, for *P. gingivalis* and 600, 600 and 300 nM for *F. nucleatum*), and 2 μL of DNA from samples. The negative control was 2 μL of sterile water [no template control (NTC)] (Water PCR grade, Roche). The samples were subjected to an initial amplification cycle of 95 °C for 10 min, followed by 45 cycles at 95 °C for 15 s and 60 °C for 1 min. Analyses were performed with a LightCycler® 480 II thermocycler (Roche). The plates used in the study was FramStar 480 of natural frame and white wells (4titude; The North Barn; Damphurst Lane, UK), sealed by QPCR Adhesive Clear Seals (4titude).

Each DNA sample was analyzed in duplicate. Quantification cycle (Cq) was determined using the provided software package (LC 480 Software 1.5; Roche). Quantification of cells by qPCR was based on standard curves. The correlation between Cq values and CFU mL^{-1} were automatically generated through the software (LC 480 Software 1.5; Roche).

2.10. Statistical analysis

The outcome variable to assess the effect of the nanoparticles on HA discs was the nano-roughness (SRa, in nm). The outcome variables to assess biofilms formed on different surfaces were micrometres (μm) of height, number of each bacterium (CFU mL^{-1}) and bacterial viability.

An experiment-level analysis was performed for each study parameter (n = 3 for each parameter studied). Shapiro–Wilk goodness-of-fit tests and distribution of data were used to assess normality. Data were expressed as means and Standard Deviation (SD). SRa, micrometres (μm) of height and bacterial viability data were compared through ANOVA and Student Newman Keuls ($p < 0.05$). To compare the effects of the material surface at different exposure times on CFU mL^{-1}, analysis of variance and post-hoc testing with T3 Dunnett´s correction was used.

Results were considered statistically significant at $p < 0.05$. A software package (IBM SPSS Statistics 22.0; IBM Corporation, Armonk, NY, USA) was used for all data analysis.

3. Results

3.1. Nano-roughness analysis of surfaces

Surface modifications by nanoparticles coating may be observed at Fig. 1A and B. Mean surface roughness was augmented after nanoparticles coating in all cases (Table 1). All surfaces loaded with the different nanoparticles showed significant increased roughness values when compared to HA controls ($p < 0.05$ in all cases), which ranged between 11 and 15 times higher after deposition of nanoparticles (Table 1).

3.2. Morphological analysis of biofilms

All five types of NPs onto the HA discs demonstrated a uniform covering (Fig. 1B). Fig. 2 depict the multispecies biofilm formation over each specimen at different times (12, 24, 48 and 72 h). During the first hours of development (12 h), test and control discs reveled individual bacterial cells and multicellular aggregates spread across the surface, with a structural organization based primarily on bacterial cell-to-cell binding (co-aggregation) (Fig. 2). Spindle-shaped rods, suggestive of *F. nucleatum* could be recognized forming a network that seemed to start the formation of the three-dimensional structure of a biofilm (Fig. 2). The only relevant differences among the specimens occurred with the Doxy-NPs discs, where very few bacteria could be recognized at their surface. The different NPs were evenly distributed onto the whole disc surface (Fig. 2).

After 24 h, higher quantities of bacteria were observed on all the discs, irrespective of their treatment, forming a thick layer of bacteria, with initial characteristics of a structured biofilm. Microbial communities interspersed with channels could be observed, suggesting that bacteria may have reached the exponential phase of growth (Fig. 2). No significant differences among the specimen discs were found in regards to the structure of the biofilm, except with biofilms on Doxy-NPs discs, which lacked an organized structure (Fig. 2). An intimate interaction between bacteria and nanoparticles could be observed (Fig. 2).

After 48 h of biofilm development, the complexity of bacterial communities increased. Biofilms over HA surfaces covered the entire disc combining a thick basal layer of cells with bacterial stacks (Fig. 2). *F. nucleatum* seemed to play a key structural role, forming the backbone network with multispecies-microcolonies adhered (Fig. 2). In Doxy-NPs discs it was not possible to detect structured biofilms (Fig. 2).

After 72 h biofilms reached the mature, stationary phase and processes of bacterial detachment could be observed in the biofilms grown onto nanoparticles covered discs (Fig. 2). In these discs few individual cells or small bacterial colonies appeared dispersed onto their surface (Fig. 2). These detached biofilms showed a similar structure to those formed onto the control discs (Fig. 3A-B), and also depicted an intimate association between bacteria and nanoparticles in particular at the bottom area of the biofilm, where coco and coco-bacilli bacteria predominate (Fig. 3A, white arrows). NPs were intimately associated to cells membranes. A higher number of NPs were found around bacteria when NPs were loaded with calcium, zinc or silver than when NPs were unloaded (Fig. 3C–H).

3.3. Biofilm vitality

After 72 h of development, CLSM analysis showed mature biofilms, with a similar structure irrespective of the characteristic of the discs (control and NPs coated discs) characterized by an irregular architecture, that combines a thick and discontinuous basal layer of bacterial cells with stacks of bacterial aggregations (Fig. 4A–F).

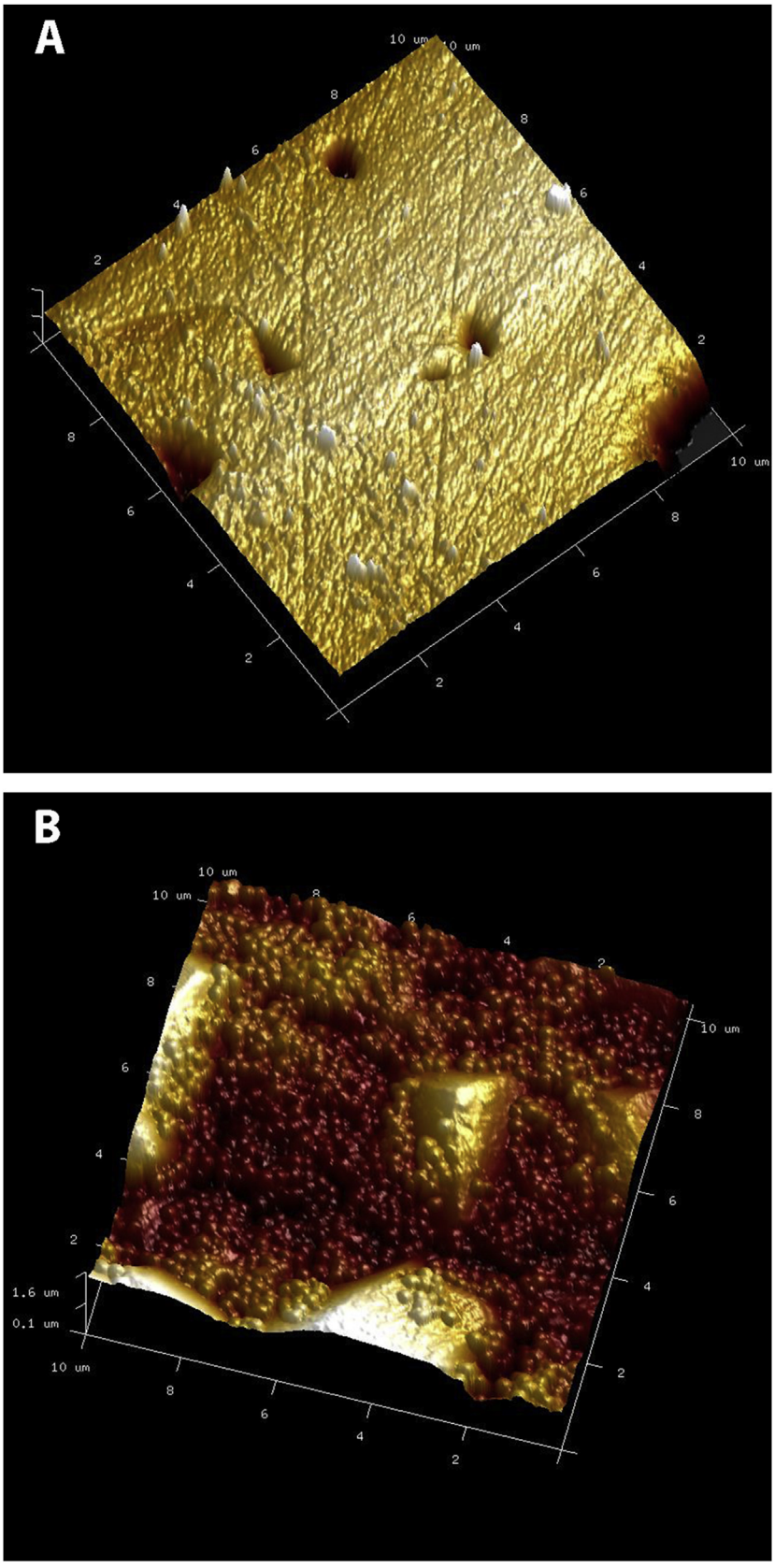

Fig. 1 – Atomic force microscopy (AFM) micrographs (10 × 10 μm), on tapping mode, of hydroxyapatite (HA) surfaces, previously treated with saliva, (A) non-coated and (B) coated with nanoparticles (NPs) doped with doxycycline. A drastic increase in roughness may be observed. Homogeneous distribution of the NPs onto the HA surface is evidenced.

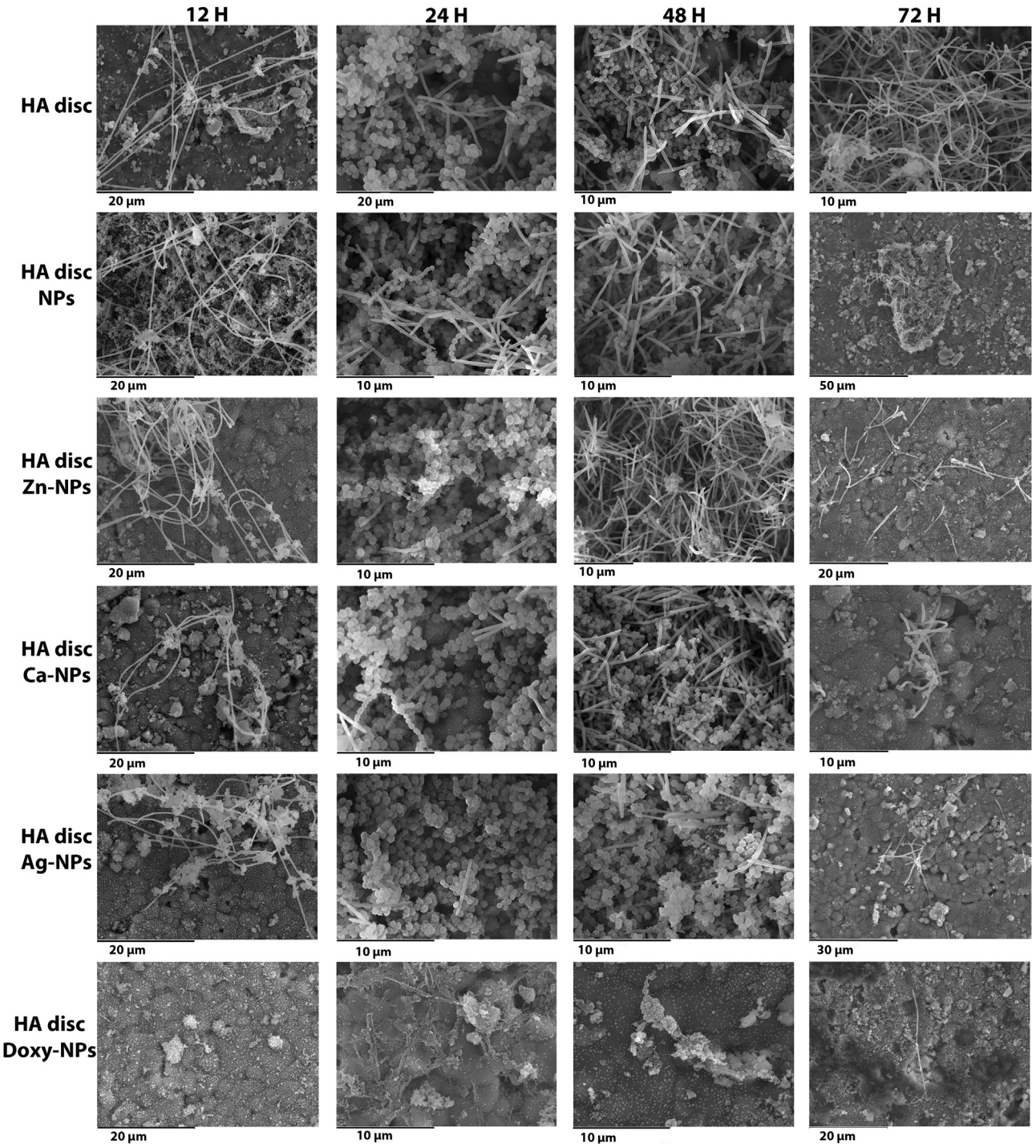

Fig. 2 – Scanning electron microscopy (SEM) of biofilms up to 72 h of development on hydroxyapatite discs (HA), previously treated with saliva, and coated with Phosphate buffer saline (PBS) as control; Nanoparticles (NPs); NPs doped with zinc; NPs doped with calcium; NPs doped with silver; and NPs doped with doxycycline. At 12 h, in all cases, bacteria appeared dispersed as individual or grouped cells, excepted in HA discs loaded with doxycycline-NPs, where very few bacteria could be recognized in the surface. Between 24 and 48 h of growth, a denser bacterial population could be observed on HA discs in all cases (treated or not with NPs) formed discontinuous layers of bacteria adhered to the studied specimens, excepted for biofilms on Doxycycline-NPs discs, where biofilm was destructed. At 72 h, while a highest density of bacteria could be observed on control discs, at NPs-coated HA discs it was not possible to find this bacterial consortium adhered to the surfaces. Solely few individual cells or small bacterial colonies appeared dispersed onto the surfaces. During the whole incubation it could be observed the different NPs homogeneously covering the HA surface and the interaction between bacteria and NPs.

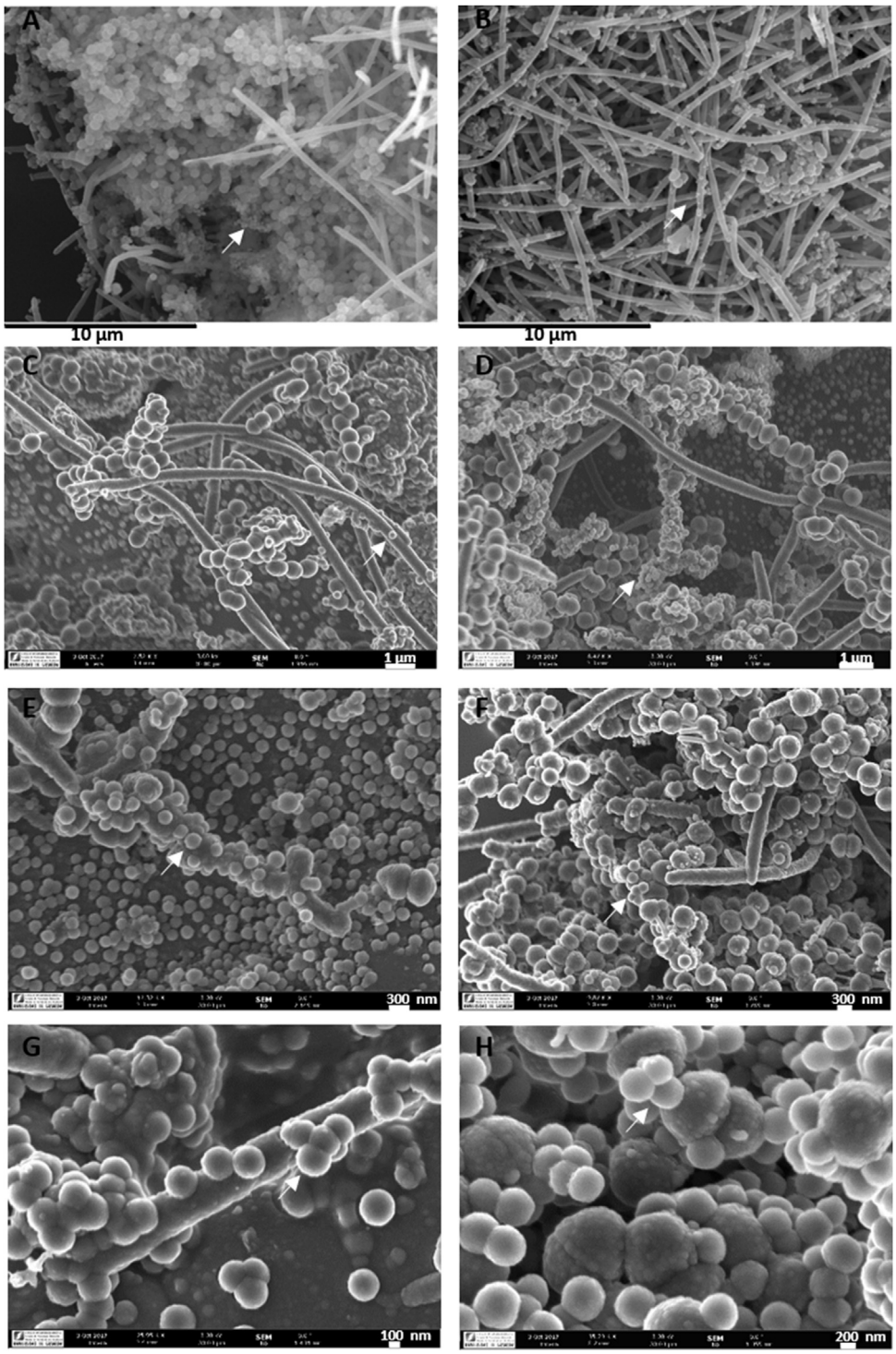

Fig. 3 – Scanning Electron Microscopy (A,B) and Field Emission Scanning Electron Microscopy (C-H) images from mature bacterial biofilms (72 h) detached from the hydroxyapatite (HA) discs. (A,B): Bacterial biofilms were detached from the HA discs and could be observed from the bottom by SEM. In all detached biofilms a dense cell community is observed, where bacteria and NPs are intimately associated, mainly in the deepest or lower zone of the biofilm, where coccoid and coco-bacillary bacteria predominate (white arrows). (C-H): 72 h detached biofilms, developed on HA surfaces coated with (C) nanoparticles (NPs); (D,E) calcium-doped NPs; (F) zinc-doped NPs and (G,H) silver-doped NPs. Bacterial biofilms were detached from the HA discs but isolated groups of bacteria may still be observed onto the surfaces. NPs are intimately associated to cells membranes. A higher number of NPs may be found around bacteria when NPs are loaded with calcium, zinc or silver NPs (white arrows). Zinc-NPs seem to induce deep changes in cells membranes, which appeared rougher and exhibit formations with different morphologies (F).

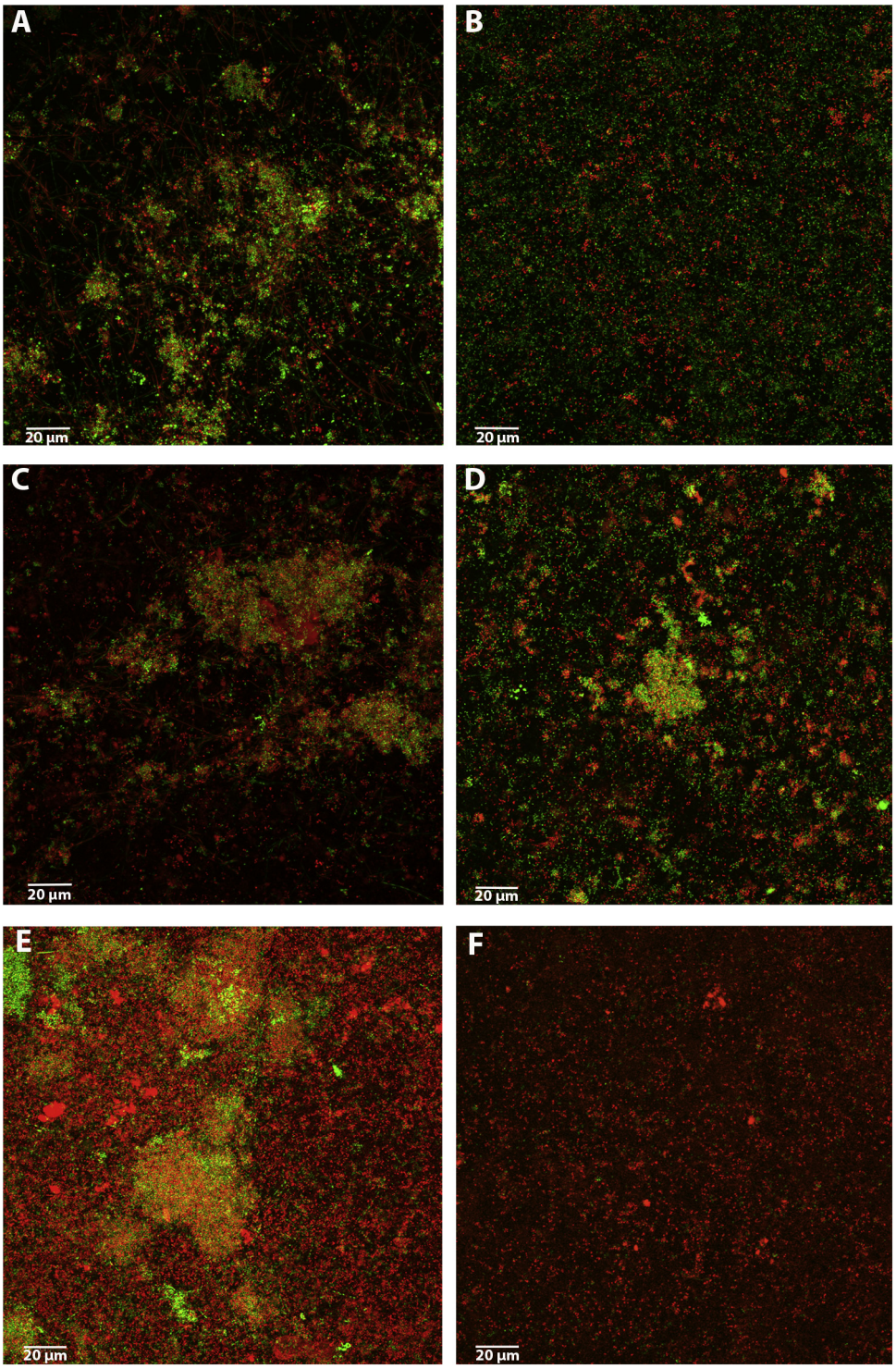

Fig. 4 – Confocal micrographs that represented a 2D maximum projection of the series along fixed axis of the biofilms after 72 h of growth on hydroxyapatite discs (HA), previously treated with saliva, and coated with (A) Phosphate buffer saline (PBS) as control; (B) Nanoparticles (NPs); (C) NPs doped with zinc; (D) NPs doped with calcium; (E) NPs doped with silver; and (F) NPs doped with doxycycline. LIVE/DEAD® BacLight™ Bacterial Viability Kit was used to assess the vitality of cells. Nanoparticles coated discs showed a decrease in cell vitality in their developed biofilms when compared to control discs (live cells in green and dead cells in red). (For interpretation of the references to color in this figure legend, the reader is referred to the web version of this article.)

Table 1 – Mean and standard deviation (SD) of surface roughness (N = 3, measured by AFM) and biofilm thickness (N = 3, measured by CLSM) for the different experimental groups. Hydroxiapatite (HA) discs treated with Posphate Buffer Saline as control, and doped with five modalities of biocompatible PolymP-*n* Active nanoparticles (NPs): NPs, NPs doped with calcium, zinc, silver and doxycycline.

	HA disc	HA disc NPs	HA disc Ca-NPs	HA disc Zn-NPs	HA disc Ag-NPs	HA disc Doxy-NPs
Mean and SD of surface roughness [nm]	11.21 (4.2)	171.32* (17.2)	188.25* (21.3)	168.9* (19.9)	158.9* (18.5)	169.5* (17.7)
Mean and SD of biofilm thickness [μm]	22.8 (7.5)	35.3 (19.7)	38.3 (18.9)	41.5 (11.8)	23.8 (3.8)	28.2 (21.9)

* Significant differences compared to control HA disc ($p < 0.05$).

Nanoparticles coated discs, however, showed a decrease in cell vitality in their developed biofilms when compared to control discs. The highest percentage of dead cells was located in the deepest zone of the biofilms, in contact with the different types of NPs. The measured death rates corresponded to 91.68% for Ca-NPs, 91.27% for Zn-NPs, 97.63% Ag-NPs, in comparison with control HA discs 45.77%. In the specimens coated with Doxy-NPs it was difficult to measure since the formed biofilms were unstructured.

3.4. *Biofilm biomass and quantitative evaluation of bacteria*

Table 2 depicts the bacterial counts (CFU mL^{-1}) for the six species at the different incubation times in the tested specimens. With time, the dynamics of bacterial growth were similar independent from the specimen. After 12 h of incubation, biofilms on HA discs treated with NPs, Zn-NPs, Ca-NPs and Ag-NPs accumulated higher number of bacteria compared with control HA discs (Table 2). These differences resulted statistically significant for *S. oralis* ($p = 0.013$) and *A. actinomycetemcomitans* ($p = 0.010$). In contrast biofilms on HA discs coated with Doxy-NPs reached a lower numbers of bacteria, when compared with the control ($p < 0.001$) (Table 2). At 24 h, all bacterial species on biofilms on HA discs treated with Doxy-NPs had significantly lower number compared with the rest of the specimens and control biofilms ($p < 0.001$) (Table 2). After 48 h of development, biofilms on NPs specimens demonstrated significant higher numbers of *V. parvula* and *A. actinomycetemcomitans* when compared to control ($p = 0.045$ and 0.017, respectively). Also, Ca-NPs related biofilms showed significant higher number for *V. parvula* ($p < 0.001$), *A. actinomycetemcomitans* ($p = 0.006$), *F. nucleatum* and *P. gingivalis* ($p = 0.005$ in both cases) compared to control biofilms. After 72 h of incubation only *S. oralis* reduced their presence on biofilms on HA discs treated with the different NPs (Table 2). Again, biofilms on HA discs coated with Doxy-NPs demonstrated significantly lower number of the six bacteria, when compared with the rest of the specimens ($p < 0.001$) (Table 2).

Derived of the analysis of specimens by CLSM, it was observed that on biofilms of 72 h of development, the area occupied by bacteria was 4.4 higher on the discs covered with NPs compared to the control HA discs. In the case of the discs covered with Zn-NPs or Ca-NPs, the increases were about 8.0 and 11.0 times respectively. Discs with Ag-NPs attained 3.1 times more biofilm than those control discs. In the case of HA discs coated with Doxy-NPs the analysis was not possible due to the unstructured architecture. Measured biofilm thicknesses are shown in Table 1.

4. Discussion

This *in vitro* investigation has shown that coating HA discs with the five modalities of PolymP-*n* Active nanoparticles significantly increased the surface nano-roughness when compared with controls. Biofilms developed on the discs coated with nanoparticles demonstrated a similar biofilm formation and dynamics, although with decreased bacterial vitality, which was more pronounced when silver and doxycycline were used. These biofilms contained a higher number of bacteria but were more susceptible to detachment when compared with biofilms formed on control discs. Doxy-NPs biofilms resulted in unstructured biofilm formation and significantly lower number of bacteria (all six species) when compared with the other nanoparticles specimens and controls.

The fact that higher number of cell counts (determined by CLSM and qPCR) were measured on nanoparticles specimens (with the exception of Doxy-NPs discs) may be explained by their increased nano-roughness facilitates initial bacterial adhesion. This process is determined by the physical interaction and the triboscopic and thermodynamic properties of the surfaces [26] and therefore, the application of nanoparticles to HA discs seems to provide a favorable environment for the initial growth of the bacterial community.

After the initial stage of biofilm formation, the subsequent exponential bacterial growth seems to depend more on biological than physical or chemical processes [27]. The formation of extracellular polysaccharides provides not only intercellular adhesion but nutrients and environmental conditions for differential bacterial growth [27,28]. In this stage, biofilms in contact to the different nanoparticles demonstrated decreased vitality than biofilms on control discs, probably due to the antiseptic potential of metal cations. Silver is the most effective antibacterial metal at low concentrations and against both gram-positive and gram-negative bacteria [18,19]. Several other metal ions (e.g. copper, magnesium, calcium, titanium, and zinc) have also displayed important antibacterial activity against a wide variety of microorganisms [29–33]. Moreover, inorganic ions and metallic oxides have extensively demonstrated antibacterial properties when being doped on nanoparticles [16–19]. In the present study, calcium release from NPs was estimated as 0.08 and 0.1 μg mL^{-1} (per mg of NPs) from 12 h up to 7 days, while the release of

Table 2 – Number of bacteria [CFU/biofilm mean (standard deviation)] of *S. oralis*, *A. naeslundii*, *V. parvula*, *F. nucleatum*, *A. actinomycetemcomitans* and *P. gingivalis* grown as multi-species biofilm *in vitro* at different times of incubation, measured by quantitative real-time polymerase chain reaction (qPCR) (N = 3 for each incubation time). Hydroxyapatite (HA) discs, previously treated with saliva, doped with Posphate Buffer Saline as control, and doped with five modalities of biocompatible PolymP-*n* Active nanoparticles (NPs): NPs, NPs doped with calcium, zinc, silver and doxycycline.

Bacteria	Time of biofilm incubation (h)	Number of bacteria [CFU/biofilm mean (standard deviation)]					
		HA disc	HA disc NPs	HA disc Ca-NPs	HA disc Zn-NPs	HA disc Ag-NPs	HA disc Doxy-NPs
So	12	5.1E + 07 (9.6E + 06)	1.6E + 08* (4.0E + 07)	1.0E + 08 (1.9E + 07)	6.7E + 07 (1.1E + 07)	1.3E + 08 (8.0E + 07)	7.0E + 04* (5.6E + 04)
	24	2.3E + 08 (4.8E + 07)	1.7E + 08 (6.5E + 07)	1.5E + 08 (8.7E + 07)	1.2E + 08 (9.8E + 07)	1.2E + 08 (7.2E + 07)	3.2E + 04* (2.7E + 04)
	48	8.5E + 07 (9.7E + 07)	1.5E + 08 (9.1E + 07)	2.0E + 08 (1.3E + 08)	1.7E + 08 (1.0E + 08)	1.3E + 08 (6.3E + 07)	1.4E + 04* (6.7E + 03)
	72	6.8E + 07 (1.6E + 07)	4.7E + 07 (5.2E + 06)	8.0E + 07 (9.9E + 06)	7.6E + 07 (2.3E + 07)	7.6E + 07 (5.8E + 07)	1.7E + 04* (8.9E + 03)
An	12	5.9E + 06 (4.5E + 06)	4.9E + 06 (3.7E + 06)	8.9E + 06 (3.6E + 06)	7.0E + 06 (4.0E + 06)	6.5E + 06 (4.0E + 06)	4.4E + 04* (8.5E + 03)
	24	1.7E + 07 (5.3E + 06)	1.9E + 07 (1.1E + 06)	1.0E + 07 (3.8E + 06)	8.8E + 06 (4.1E + 06)	9.8E + 06 (1.4E + 06)	5.4E + 04* (1.3E + 04)
	48	2.2E + 07 (6.6E + 06)	2.2E + 07 (9.1E + 05)	2.1E + 07 (1.7E + 06)	2.1E + 07 (2.3E + 06)	2.4E + 07 (5.1E + 06)	4.5E + 04* (3.4E + 03)
	72	7.8E + 06 (6.0E + 05)	5.4E + 06 (1.1E + 06)	7.7E + 06 (2.9E + 06)	9.9E + 06 (3.5E + 06)	9.2E + 06 (5.6E + 06)	3.7E + 04* (1.5E + 04)
Vp	12	3.8E + 07 (2.2E + 07)	5.8E + 07 (1.1E + 07)	3.5E + 07 (1.3E + 07)	3.6E + 07 (2.0E + 06)	4.3E + 07 (2.5E + 07)	4.1E + 04* (3.1E + 04)
	24	8.2E + 07 (4.2E + 07)	1.1E + 08 (1.1E + 07)	1.3E + 08 (5.3E + 07)	5.2E + 07 (2.9E + 07)	5.6E + 07 (1.4E + 07)	1.8E + 04* (3.7E + 03)
	48	4.1E + 07 (3.0E + 07)	9.5E + 07* (3.0E + 07)	1.4E + 08* (2.4E + 07)	9.1E + 07 (2.2E + 07)	6.7E + 07 (9.2E + 06)	3.4E + 04* (2.0E + 04)
	72	4.7E + 07 (1.9E + 07)	2.1E + 07 (1.4E + 07)	4.5E + 07 (1.6E + 07)	4.1E + 07 (2.0E + 07)	1.9E + 07 (1.3E + 07)	1.8E + 04* (1.1E + 04)
Fn	12	8.1E + 06 (6.0E + 06)	1.3E + 07 (3.5E + 06)	1.3E + 07 (6.5E + 06)	1.3E + 07 (3.7E + 06)	1.6E + 07 (8.5E + 06)	1.4E + 05* (3.2E + 04)
	24	4.4E + 07 (2.8E + 07)	3.6E + 07 (1.2E + 06)	4.1E + 07 (1.8E + 07)	3.4E + 07 (7.6E + 06)	3.0E + 07 (1.3E + 07)	2.2E + 05* (6.9E + 04)
	48	2.1E + 07 (1.4E + 07)	4.9E + 07 (1.4E + 07)	6.3E + 07* (1.8E + 07)	4.2E + 07 (1.3E + 07)	2.5E + 07 (5.8E + 06)	1.0E + 05* (3.5E + 04)
	72	1.9E + 07 (2.1E + 06)	1.7E + 07 (3.0E + 06)	2.4E + 07 (2.7E + 07)	3.5E + 07 (1.1E + 07)	2.6E + 07 (2.1E + 07)	4.4E + 04* (1.2E + 04)
Aa	12	5.7E + 06 (1.8E + 06)	1.7E + 07* (2.8E + 06)	8.9E + 06 (2.8E + 06)	9.2E + 06 (1.7E + 06)	1.2E + 07 (4.8E + 06)	3.3E + 05* (1.8E + 05)
	24	1.3E + 07 (4.2E + 06)	2.6E + 07 (4.6E + 06)	3.9E + 07 (1.6E + 07)	2.4E + 07 (4.8E + 06)	2.0E + 07 (7.6E + 06)	5.5E + 05* (8.9E + 04)
	48	1.1E + 07 (3.6E + 06)	3.5E + 07* (8.4E + 06)	3.9E + 07* (3.3E + 07)	2.3E + 07 (6.4E + 06)	2.8E + 07 (1.7E + 07)	9.9E + 04* (8.4E + 04)
	72	1.7E + 07 (4.0E + 06)	1.5E + 07 (2.5E + 05)	2.5E + 07 (2.0E + 06)	2.4E + 07 (5.2E + 06)	2.2E + 07 (1.5E + 07)	1.4E + 05* (4.3E + 04)
Pg	12	4.6E + 07 (3.3E + 07)	7.6E + 07 (1.9E + 07)	7.5E + 07 (3.6E + 07)	7.4E + 07 (2.0E + 07)	9.1E + 07 (4.6E + 07)	9.1E + 05* (2.0E + 05)
	24	2.4E + 08 (1.5E + 08)	2.0E + 08 (6.4E + 06)	2.2E + 08 (9.6E + 07)	1.9E + 08 (4.0 + 07)	1.7E + 08 (6.6E + 07)	1.4E + 06* (4.3E + 05)
	48	1.2E + 08 (7.5E + 07)	2.6E + 08 (7.1E + 07)	3.4E + 08* (9.4E + 07)	2.3E + 08 (6.8 + 07)	1.4E + 08 (3.1E + 07)	6.6E + 05* (2.3E + 05)
	72	1.0E + 08 (1.1E + 07)	7.3E + 07 (3.9 E + 07)	1.3E + 08 (1.4E + 07)	1.9E + 08 (5.6E + 07)	1.4E + 08 (1.1E + 08)	3.0E + 05* (7.7E + 04)

* Significant differences compared to control HA disc ($p < 0.05$).

zinc was 0.02 $\mu g\,mL^{-1}$ (per mg of NPs) at the same time-points. Cumulative liberation of both ions was 30% for calcium and 0.3% for zinc after 48 h [24]. FESEM observations revealed that Zinc-NPs induced deep changes in cells membranes, being thicker and adopting different morphologies (Fig. 3F). Zinc ions also markedly enhanced the adhesion and accumulation of salivary and serum proteins on bacteria membranes and inhibited their coaggregation when growing on biofilms, as it

has been described previously [34]. The FESEM images also depicted a stronger interaction between loaded NPs and bacteria membranes when compared to non-loaded NPs (Fig. 3). Fig. 3D–H (loaded NPs) show increased number of NPs adhered to bacteria membranes compared to non-loaded NPs (Fig. 3C). These findings can be explained by the different attraction between NPs to bacteria membranes dependent on the surfaces charges. NPs doped with cationic groups (calcium, zinc or silver) will interact easily with bacterial cell membranes exhibiting anionic charges (zeta potential around −20 mV at pH = 7) [35]. On the contrary, since non-loaded NPs are anionic (potential zeta is −41 ± 5 mV at pH = 7) [11] will not be attracted to bacterial cell membranes.

At the stationary phase, in nanoparticles specimen biofilms contained a higher number of bacteria, although demonstrating higher rates of mortality, and were more susceptible to detachment when compared with biofilms formed on control discs. One possible explanation for this increased growth may be related to the presence of functional groups in the nanoparticles, which facilitate protein binding and therefore, decrease the sites available for *quorum sensing* molecules [36,37]. It is well studied that the oral bacteria used in this *in vitro* biofilm system produce and release to the external environment a series of molecules called autoinducers [38–40], proteins containing amino groups (i.e. NH_2) that will form covalent peptide bonds with carboxylate (i.e. $-COO^-$) sites in the nanoparticles, thus facilitating protein binding and preventing bacteria to sense when a *quorum* is reached, and hence, *quorum sensing*-controlled genes will not be activated. Increased protein binding affinity of tested nanoparticles has been previously demonstrated with dentin collagen and fibrin [15,41]. Rasmussen and Givskov has also reported that uncontrolled growth of bacteria will lead to thick biofilms more prone to detachment [36]. This effect of detachment was clearly observed in the 72 h biofilms associated with the different types of nanoparticles. The detachment was produced at the bottom of the biofilms, between the substrate and the first colonizers layer. So, it is possible that nanoparticles at the conditioning layer moreover act as a weak link interposed between the HA surface and the bacteria, promoting also the bacterial death at the bottom (observed by CLSM) the breakdown of the biofilm.

Ag-NPs have been used extensively as anti-bacterial agents in a number of healthcare applications, although there are few reports on their use against oral bacteria, and in particular periodontal pathogens [42–45]. In the present study, NPs doped with silver demonstrated an effective biocide activity against the bacterial biofilm, displaying a broad-spectrum antibacterial effect that included both Gram-negative and Gram-positive bacteria [43,46,47]. However, only the discs doped with Doxy-NPs resulted in a significant reduction in viable bacterial counts cells and vitality. Although doxycycline has a clear bactericidal activity through the inhibition of the microbial protein synthesis [20–22], high doses are needed to penetrate the biofilm, with reported concentrations of approximately 250 times greater than what may be to destroy the same strains grown planktonically [39]. The tested Doxy-NPs discs exhibited a controlled release of doxycycline at least over 28 days. For each mg of NPs 121, 106 and 46 $\mu g\,ml^{-1}$ of doxycycline was liberated at 12, 24 and 48 h respectively, with the antibiotic release maintained above 20 $\mu g\,ml^{-1}$ until 7 days [24]. Since bacterial susceptibility to doxycycline is around 0.1 a 0.2 $\mu g\,ml^{-1}$ [21], the released concentrations of doxycycline from NPs was above to the antibacterial effective dose. Doxy-NPs have been previously shown to exert antibacterial activity in planktonic cultures against *P. gingivalis* [24]. Doxycycline at a concentration between 0.5 and 1 $\mu g\,ml^{-1}$ is bactericidal against different *P. gingivalis* strains [48], and between 0.1 and 6.0 $\mu g\,ml^{-1}$ is effective against *P. gingivalis* and other putative periodontal pathogens [49,50]. Furthermore, this release occurred from the bottom of the biofilm, thus being bactericidal for the early colonizers responsible for the biofilm anchorage [21], what may explain the lack of structure in these biofilms formed on Doxy-NPs discs.

The results reported in this study should be interpreted with caution due to the *in vitro* nature of this investigation. Future research in animal models and other relevant *in vivo* settings should test the real impact of this biocompatible PolymP-*n* Active nanoparticles could as an effective antibacterial therapy for the treatment of periodontitis. Furthermore, the use of these nanoparticles should be tested as coatings of biomaterials currently use in periodontal regeneration to assess their adjunctive effect to improve regenerative outcomes.

5. Conclusion

This *in vitro* investigation has demonstrated that coating surfaces with nanoparticles and metallic ions will have an impact on biofilm formation by reducing its vitality and by weakening the attachment between the matrix and the first colonizers, thus being more susceptible to detachment.

Acknowledgements

Project MAT2017-85999-P MINECO/AEI/FEDER/UE was supported by the Ministry of Economy and Competitiveness and European Regional Development Fund; and Extraordinary Chair of DENTAID-UCM. Microscopy analyses were carried out at the Centre of Microscopy and Cytometry from the University Complutense of Madrid, Spain and at the Centre of Scientific Instrumentation from the University of Granada, Spain.

REFERENCES

[1] Cortellini P, Tonetti MS. Focus on intrabony defects: guided tissue regeneration. Periodontol 2002 2000;22:104–32.
[2] Larsson L, Decker AM, Nibali L, Pilipchuk SP, Berglundh T, Giannobile WV. Regenerative medicine for periodontal and peri-implant diseases. J Dent Res 2016;95:255–66.
[3] Heitz-Mayfield L, Tonetti MS, Cortellini P, Lang NP. European Research Group on P. Microbial colonization patterns predict the outcomes of surgical treatment of intrabony defects. J Clin Periodontol 2006;33:62–8.
[4] Machtei EE, Oettinger-Barak O, Peled M. Guided tissue regeneration in smokers: effect of aggressive anti-infective therapy in Class II furcation defects. J Periodontol 2003;74:579–84.

[5] Sander L, Frandsen EV, Arnbjerg D, Warrer K, Karring T. Effect of local metronidazole application on periodontal healing following guided tissue regeneration. Clinical findings. J Periodontol 1994;65:914–20.
[6] Stavropoulos A, Karring ES, Kostopoulos L, Karring T. Deproteinized bovine bone and gentamicin as an adjunct to GTR in the treatment of intrabony defects: a randomized controlled clinical study. J Clin Periodontol 2003;30:486–95.
[7] Nowzari H, Slots J. Microorganisms in polytetrafluoroethylene barrier membranes for guided tissue regeneration. J Clin Periodontol 1994;21:203–10.
[8] Abou Neel EA, Bozec L, Perez RA, Kim HW, Knowles JC. Nanotechnology in dentistry: prevention, diagnosis, and therapy. Int J Nanomed 2015;10:6371–94.
[9] Jain N, Jain GK, Javed S, Iqbal Z, Talegaonkar S, Ahmad FJ, et al. Recent approaches for the treatment of periodontitis. Drug Discov Today 2008;13:932–43.
[10] Walmsley GG, McArdle A, Tevlin R, Momeni A, Atashroo D, Hu MS, et al. Nanotechnology in bone tissue engineering. Nanomedicine 2015;11:1253–63.
[11] Osorio R, Alfonso-Rodriguez CA, Medina-Castillo AL, Alaminos M, Toledano M. Bioactive polymeric nanoparticles for periodontal therapy. PLoS One 2016;11:e0166217.
[12] Sahoo SK, Parveen S, Panda JJ. The present and future of nanotechnology in human health care. Nanomedicine 2007;3:20–31.
[13] Ozak ST, Ozkan P. Nanotechnology and dentistry. Eur J Dent 2013;7:145–51.
[14] Medina-Castillo AL, Fernandez-Sanchez JF, Segura-Carretero A, Fernandez-Gutierrez A. Micrometer and submicrometer particles prepared by precipitation polymerization: thermodynamic model and experimental evidence of the relation between Flory's parameter and particle size. Macromolecules 2010;43:5804–13.
[15] Osorio R, Osorio E, Medina-Castillo AL, Toledano M. Polymer nanocarriers for dentin adhesion. J Dent Res 2014;93:1258–63.
[16] Munchow EA, Albuquerque MT, Zero B, Kamocki K, Piva E, Gregory RL, et al. Development and characterization of novel ZnO-loaded electrospun membranes for periodontal regeneration. Dent Mater 2015;31:1038–51.
[17] Munchow EA, Pankajakshan D, Albuquerque MT, Kamocki K, Piva E, Gregory RL, et al. Synthesis and characterization of CaO-loaded electrospun matrices for bone tissue engineering. Clin Oral Investig 2016;20:1921–33.
[18] Fabrega J, Luoma SN, Tyler CR, Galloway TS, Lead JR. Silver nanoparticles: behaviour and effects in the aquatic environment. Environ Int 2011;37:517–31.
[19] Baalousha M, Nur Y, Romer I, Tejamaya M, Lead JR. Effect of monovalent and divalent cations, anions and fulvic acid on aggregation of citrate-coated silver nanoparticles. Sci Total Environ 2013;45:4–455, 119–31.
[20] Pascale D, Gordon J, Lamster I, Mann P, Seiger M, Arndt W. Concentration of doxycycline in human gingival fluid. J Clin Periodontol 1986;13:841–4.
[21] Kim TS, Burklin T, Schacher B, Ratka-Kruger P, Schaecken MT, Renggli HH, et al. Pharmacokinetic profile of a locally administered doxycycline gel in crevicular fluid, blood, and saliva. J Periodontol 2002;73:1285–91.
[22] Demirel K, Baer PN, McNamara TF. Topical application of doxycycline on periodontally involved root surfaces in vitro: comparative analysis of substantivity on cementum and dentin. J Periodontol 1991;62:312–6.
[23] Sanchez MC, Llama-Palacios A, Blanc V, Leon R, Herrera D, Sanz M. Structure, viability and bacterial kinetics of an in vitro biofilm model using six bacteria from the subgingival microbiota. J Periodontal Res 2011;46:252–60.
[24] Toledano-Osorio M, Babu JP, Osorio R, Medina-Castillo AL, Garcia-Godoy F, Toledano M. Modified polymeric nanoparticles exert in vitro antimicrobial activity against oral bacteria. Materials (Basel) 2018:11.
[25] Sanchez MC, Llama-Palacios A, Fernandez E, Figuero E, Marin MJ, Leon R, et al. An in vitro biofilm model associated to dental implants: structural and quantitative analysis of in vitro biofilm formation on different dental implant surfaces. Dent Mater 2014;30:1161–71.
[26] Ionescu AC, Hahnel S, Cazzaniga G, Ottobelli M, Braga RR, Rodrigues MC, et al. Streptococcus mutans adherence and biofilm formation on experimental composites containing dicalcium phosphate dihydrate nanoparticles. J Mater Sci Mater Med 2017;28:108.
[27] Garrett TR, Bhakoo M, Zhang ZB. Bacterial adhesion and biofilms on surfaces. Prog Nat Sci 2008;18:1049–56.
[28] Dunne Jr WM. Bacterial adhesion: seen any good biofilms lately? Clin Microbiol Rev 2002;15:155–66.
[29] Goudouri OM, Kontonasaki E, Lohbauer U, Boccaccini AR. Antibacterial properties of metal and metalloid ions in chronic periodontitis and peri-implantitis therapy. Acta Biomater 2014;10:3795–810.
[30] Sawai J, Yoshikawa T. Quantitative evaluation of antifungal activity of metallic oxide powders (MgO, CaO and ZnO) by an indirect conductimetric assay. J Appl Microbiol 2004;96:803–9.
[31] Kasraei S, Sami L, Hendi S, Alikhani MY, Rezaei-Soufi L, Khamverdi Z. Antibacterial properties of composite resins incorporating silver and zinc oxide nanoparticles on Streptococcus mutans and Lactobacillus. Restor Dent Endod 2014;39:109–14.
[32] Shalumon KT, Anulekha KH, Nair SV, Nair SV, Chennazhi KP, Jayakumar R. Sodium alginate/poly(vinyl alcohol)/nano ZnO composite nanofibers for antibacterial wound dressings. Int J Biol Macromol 2011;49:247–54.
[33] Roy A, Gauri SS, Bhattacharya M, Bhattacharya J. Antimicrobial activity of caO nanoparticles. J Biomed Nanotechnol 2013;9:1570–8.
[34] Tamura M, Ochiai K. Zinc and copper play a role in coaggregation inhibiting action of Porphyromonas gingivalis. Oral Microbiol Immunol 2009;24:56–63.
[35] Cowan MM, Van der Mei HC, Stokroos I, Busscher HJ. Heterogeneity of surfaces of subgingival bacteria as detected by zeta potential measurements. J Dent Res 1992;71:1803–6.
[36] Rasmussen TB, Givskov M. Quorum-sensing inhibitors as anti-pathogenic drugs. Int J Med Microbiol 2006;296:149–61.
[37] Marsh PD, Moter A, Devine DA. Dental plaque biofilms: communities, conflict and control. Periodontol 2000;2011(55):16–35.
[38] Frias J, Olle E, Alsina M. Periodontal pathogens produce quorum sensing signal molecules. Infect Immun 2001;69:3431–4.
[39] Hojo K, Nagaoka S, Ohshima T, Maeda N. Bacterial interactions in dental biofilm development. J Dent Res 2009;88:982–90.
[40] Kolenbrander PE, Andersen RN, Blehert DS, Egland PG, Foster JS, Palmer Jr RJ. Communication among oral bacteria. Microbiol Mol Biol Rev 2002;66:486–505, table of contents.
[41] Scionti G, Rodriguez-Arco L, Lopez-Lopez MT, Medina-Castillo AL, Garzon I, Alaminos M, et al. Effect of functionalized PHEMA micro- and nano-particles on the viscoelastic properties of fibrin-agarose biomaterials. J Biomed Mater Res A 2018;106:738–45.
[42] Marassi V, Di Cristo L, Smith SGJ, Ortelli S, Blosi M, Costa AL, et al. Silver nanoparticles as a medical device in healthcare settings: a five-step approach for candidate screening of coating agents. R Soc Open Sci 2018;5:171113.

[43] Tran QH, Nguyen VQ, Le AT. Silver nanoparticles: synthesis, properties, toxicology, applications and perspectives. Adv Nat Sci Nanosci 2013:4.
[44] Halkai KR, Mudda JA, Shivanna V, Rathod V, Halkai RS. Evaluation of antibacterial efficacy of biosynthesized silver nanoparticles derived from fungi against endo-perio pathogens Porphyromonas gingivalis, Bacillus pumilus, and Enterococcus faecalis. J Conserv Dent 2017;20:398–404.
[45] Lu Z, Rong K, Li J, Yang H, Chen R. Size-dependent antibacterial activities of silver nanoparticles against oral anaerobic pathogenic bacteria. J Mater Sci Mater Med 2013;24:1465–71.
[46] Sondi I, Salopek-Sondi B. Silver nanoparticles as antimicrobial agent: a case study on E. coli as a model for Gram-negative bacteria. J Colloid Interface Sci 2004;275:177–82.
[47] Neal AL. What can be inferred from bacterium-nanoparticle interactions about the potential consequences of environmental exposure to nanoparticles. Ecotoxicology 2008;17:362–71.
[48] Larsen T. Susceptibility of Porphyromonas gingivalis in biofilms to amoxicillin, doxycycline and metronidazole. Oral Microbiol Immun 2002;17:267–71.
[49] Slots J, Rams TE. Antibiotics in periodontal therapy — advantages and disadvantages. J Clin Periodontol 1990;17:479–93.
[50] Larsen T. In vitro release of doxycycline from bioabsorbable materials and acrylic strips. J Periodontol 1990;61:30–4.